Materials Today Bio 25 (2024) 100960

Contents lists available at ScienceDirect

Materials Today Bio

journal homepage: www.journals.elsevier.com/materials-today-bio

Au nanozyme-based multifunctional hydrogel for inflammation visible monitoring and treatment

Yunjing Jiang, Yuyu Cao, Jie Wu, Rongxian Bai, Shufan Wan, Lei Dai, Jiangtao Su, Hongmei Sun *

Collaborative Grant-in-Aid of the HBUT National "111" Center for Cellular Regulation and Molecular Pharmaceutics, Key Laboratory of Fermentation Engineering (Ministry of Education), Key Laboratory of Industrial Microbiology in Hubei, Cooperative Innovation Center of Industrial Fermentation (Ministry of Education & Hubei Province), School of Bioengineering and Food, Hubei University of Technology, Wuhan, 430068, China

A R T I C L E I N F O

Keywords:
Gold nanoclusters
Multifunctional hydrogel
Inflammation
Visible monitoring
Wound healing

A B S T R A C T

Chronic inflammation can delay wound healing, eventually leading to tissue necrosis and even cancer. Developing real-time intelligent inflammation monitoring and treatment to achieve effective wound management is important to promote wound healing. In this study, a smart multifunctional hydrogel (Hydrogel@Au NCs&DG) was proposed to monitor and treat the wound inflammation. It was prepared by mixing 3-carboxy-phenylboronic acid modified chitosan (CS-cPBA), β-glycerophosphate (β-GP), albumin-protected gold nanoclusters (BSA-Au NCs), and dipotassium glycyrrhizinate (DG) about 10 s. In this hydrogel, CS-cPBA and β-GP are crosslinked together by boric acid ester bond and hydrogen bond to form the main hydrogel network, endowing the hydrogel with self-healing and injectable properties to adapt irregular wounds. Importantly, the as-prepared hydrogel with good biocompatibility and excellent adhesion property could directly determine the H_2O_2 to monitor the wound microenvironment by visible fluorescence change of BSA-Au NCs and then guide the frequency of dressing change to eliminate inflammation. The results demonstrated that the as-prepared smart hydrogel could be expected to serve as an intelligent wound dressing to promote inflammation-infected wound healing.

1. Introduction

As the largest organ of human body, skin is the first line of defense against external invasion. Due to direct contact with the external environment, skin is easily damaged [1]. In order to treat skin trauma, various wound dressings have been developed, including gauze, film, foam, nanofiber, colloid, hydrogel, and so on [2–4]. Among these materials, hydrogel as a three-dimensional network composed of physical or chemical cross-linking bonds has attracted the wide interest of scientists [5–7]. Benefiting from the special structure and high water content, hydrogel shows excellent oxygen permeability and exudate absorption capacity, and thus provides a moist environment for the wound interface [8,9].

Chitosan (CS) as a natural polymer with biocompatibility, antibacterial ability, and adhesion is widely used for hydrogel preparation [10–15]. However, single chitosan-based hydrogel dressing could not meet the wound management in the clinic because of the complex microenvironment of the wound sites. It is highly demanded to develop multifunctional hydrogels. Nowadays, self-healing and injectable hydrogels have become a hot research area as they can avoid bacterial invasion caused by material damage and fit irregular wounds due to the characteristic of reversible sol-gel transition [16–18]. β-glycerophosphate (β-GP) is an organic compound naturally existing in human body, which has been used as an osteogenic supplement for culturing human bone marrow stem cells. It has good biocompatibility and water solubility, and could form multifunctional hydrogel with chitosan through hydrogen bonding, ionic bonding, and hydrophobic interaction [19–21].

Although great progress has been made with the development of hydrogel, design and exploration of smart wound dressings are still a challenge because of the complex process of wound healing. For example, many endogenous and exogenous adverse factors can destroy the physiological healing process, especially the inflammatory stage [22]. In the inflammatory stage, neutrophils and macrophages reach the injury site through chemotaxis, releasing a large number of superoxide anion free radicals, which are converted into reactive oxygen species

* Corresponding author.
E-mail address: hmsunqi@163.com (H. Sun).

https://doi.org/10.1016/j.mtbio.2024.100960
Received 21 October 2023; Received in revised form 10 January 2024; Accepted 15 January 2024
Available online 26 January 2024

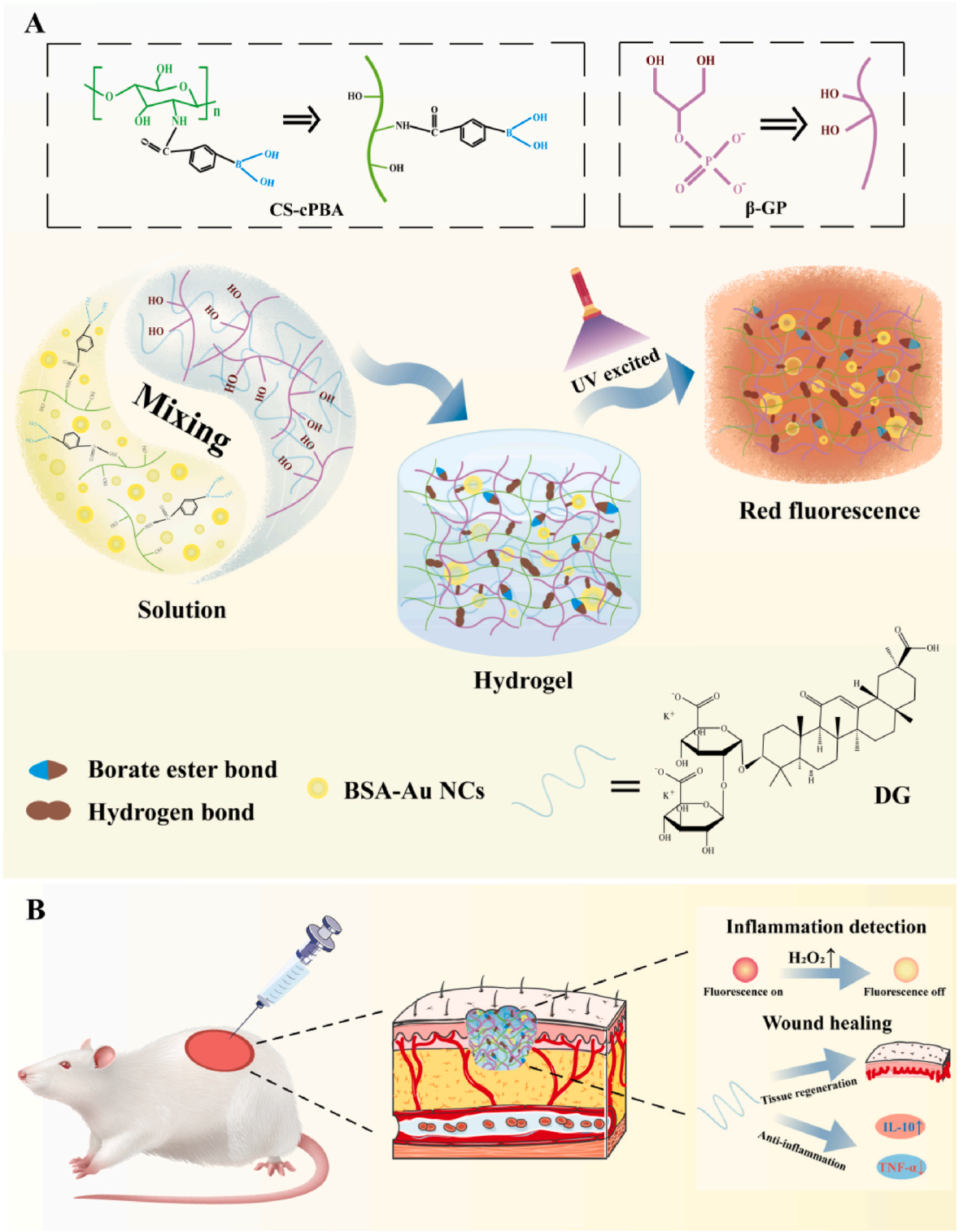

Scheme 1. (A) Formation process of Hydrogel@Au NCs&DG and (B) the mechanism of detecting inflammation and promoting wound healing.

under the action of superoxide dismutase [23,24]. Low concentration of reactive oxygen species can remove bacteria from the wound, while excessive inflammation will release a large number of reactive oxygen species, produce oxidative stress reaction, hinder angiogenesis and granulation tissue formation, finally lead to slow wound healing [25–27]. As the main member of reactive oxygen species, hydrogen peroxide (H_2O_2) plays a vital role in the process of wound healing [28,29]. When the concentration exceeds 500 μM, it will kill cells, prevent the formation of connective tissue, and lead to inflammatory diseases [30,31]. Therefore, detecting the concentration of hydrogen peroxide at the wound is important to monitor the inflammation and thus to guide the use of wound dressing.

At present, there are many sensitive methods to detect hydrogen peroxide, including enzyme-catalyzed reaction detection or fluorescence labeling [32,33]. In order to find potential substitutes, various nanoparticles with biological enzyme mimicry activity (nano-enzyme)

have been studied, such as platinum, Prussian blue, and iron oxide nanoparticles [34–36]. Although the above materials have shown good hydrogen peroxide induction, most of them can not be used for testing mammalian cells owing to their toxicity or complicated fabrication process. Currently, it is reported that bovine serum albumin-protected gold nanoclusters (BSA-Au NCs) with bright red fluorescence, facile approach, and high biocompatibility would be an ideal candidate for detection of H_2O_2 in human body [37]. Apart from monitoring the degree of wound inflammation, it is also very important to diminish inflammation and prevent the wound from deteriorating continuously. Dipotassium glycyrrhizinate (DG) is a water-soluble salt of glycyrrhizic acid extracted from licorice root. It is widely used in medicines and cosmetics due to the functions of anti-allergy, anti-tumor, and anti-inflammation. The most interesting is that it can promote the growth of granulation tissue and induce the reorganization of extracellular matrix dermis, thus promoting wound healing [38,39].

Based on the above consideration, herein, we prepared an injectable smart hydrogel (Hydrogel@Au NCs&DG) for monitoring and treatment of wound inflammation in situ. The as-prepared hydrogel was obtained by mixing 3-carboxy-phenylboronic acid modified chitosan (CS-cPBA), β-glycerophosphate (β-GP), BSA-Au NCs, and DG together about 10 s. In this hydrogel, CS-cPBA and β-GP were crosslinked together by boric acid ester bond (a dynamic and reversible chemical bond) and hydrogen bond to form the main hydrogel network [40], endowing the hydrogel with self-healing and injectable properties. Importantly, BSA-Au NCs with visible fluorescence in the hydrogel can monitor the degree of wound inflammation by the detection of concentration of H_2O_2, and DG was released to reduce the inflammatory reaction to promote wound healing (Scheme 1). It would provide a new platform for the preparation of smart wound dressing.

2. Materials and methods

2.1. Materials

3-carboxyphenyl boric acid (3-cPBA, MW 165.94), Chitosan (CS, deacetylation degree ≥95 %, viscosity 100–200 mpa·s, MW 700–800 kDa), β-glycerophosphate sodium (β-GP), dipotassium glycyrrhizinate (DG, MW 899.12), acetic acid (HAC), 1-(3-dimethylaminopropyl)-3-ethyl carbodiimide hydrochloride (EDC), N-hydroxysuccinimide (NHS) were acquired from Macklin (Shanghai, China). Sodium citrate anticoagulates rabbit blood was purchased from Nanjing Senbega Biotechnology Co., Ltd. Mouse fibroblast L929 was from Procell, China. Other chemical reagents are analytical pure, purchased from China National Pharmaceutical Group Chemical Reagent Co., Ltd.

Kunming mice (25–30 g, female) were provided by Huazhong Agricultural University (Wuhan, China). All animal experiments were conducted in accordance with the National Research Council's Guidelines for the Care and Use of Experimental Animals, and were approved by the Animal Ethics Committee of Hubei University of Technology. The protocol approval number of animal experiment is HBUT20230079.

2.2. Preparation of CS-cPBA

3-carboxyphenyl boric acid (3-cPBA) (206.2 mg) and NHS (49.32 mg) were dissolved in 24 mL of methanol and stirred at room temperature for 20 min. Next, EDC (66.52 mg) and chitosan solution (0.2 g of chitosan powder dissolved in 24 mL of 0.3 % HAC) were added to the mixed solution at pH = 5–6, then stirred at room temperature for 24 h. Subsequently, the product was dialyzed for 48 h and water was changed every 4 h, before lyophilization. The grafting rate of CS-cPBA was calculated according to UV–vis absorbance (ABS) standard curve of 3-cPBA at 275 nm.

2.3. Preparation of BSA-Au NCs

Bovine serum albumin (BSA)-protected gold nanoclusters were synthesized according to the method described previously [41,42]. Briefly, the $HAuCl_4$ aqueous solution (5 mL, 10 mM) was introduced into the BSA solution (5 mL, 50 mg/mL) with rapid agitation, and after 2 min, the NaOH solution (0.5 mL, 1 M) was added to the mixed solution until pH = 12. All experiments were carried out in 37 °C water bath and stirred vigorously for 12 h in darkness. The product was dialyzed in ultrapure water for 24 h and the water was changed every 4 h. Finally, the product after dialysis was freeze-dried to obtain BSA-Au NCs for further use.

2.4. H_2O_2 determination by BSA-Au NCs

5 mg/mL of BSA-Au NCs were incubated with different concentrations of hydrogen peroxide (0–500 μM) for 20 min at room temperature, then the fluorescence intensity of BSA-Au NCs (Ex./Em.506/660 nm) was determined by fluorescence spectrometer.

2.5. Preparation and characterization of CS-cPBA/β-GP hydrogels

The CS-cPBA solution with concentration of 4 % w/v was mixed with 60 % w/v β-GP solution. After 10 s, the CS-cPBA/β-GP hydrogel (named Control hydrogel) was formed. Then the rheological and swelling properties were evaluated. The experimental details have been provided in the experimental section in the Supporting Information.

2.6. Drug release from hydrogels

Hydrogel@Au NCs&DG (1.25 mL) was loaded into dialysis bags (MWCO = 14000, n = 3), submerged in phosphate-buffered saline (100 mL of PBS) at pH 7.4, then external dialyzate (2 mL) was detected at specific time intervals and timely supplemented the same amount of PBS. The release of dipotassium glycyrrhizinate (DG) was evaluated by UV–vis spectroscopy.

2.7. In vitro biocompatibility examination

The hydrogel-mediated hemolysis was evaluated using sodium lysate anticoagulant rabbit blood. The cell compatibility of the hydrogel was tested on mouse fibroblast L929, and the growth and migration of the hydrogel-treated cells were evaluated by cell scratch test. Details of the experiment are shown in the support information.

2.8. In vitro anti-inflammatory assay

Raw 264.7 macrophages were exposed to DMEM medium containing LPS (10 μg/mL) for 2 h and then co-incubated with hydrogel extract for 24 h. Cytotoxicity was assessed by MTT assay, and IL-10 and TNF-α levels were assessed by ELISA.

2.9. In vivo wound healing assay

Female Kunming mice (weight: 25–30 g) aged 4–5 weeks were randomly divided into 6 groups (n = 5), namely, Blank, Hydrosorb gel, Control hydrogel, Hydrogel@Au NCs, Hydrogel@DG and Hydrogel@Au NCs&DG. All mice were anesthetized by intraperitoneal injection of 100 μL of 1.5 % pentobarbital solution under sterile conditions. After anesthesia, a sterile scalpel was used to make a circular wound of 10 mm in diameter on the back of each mouse. An equal amount of hydrogel (1.25 mL) was applied to the wound surface postoperatively. Wound healing was assessed at 0, 3, 5, and 10 days post-traumatic. Wound tissue was cut with a scalpel on days 5 and 10, soaked in tissue-fixing fluid, and stained with Hematoxylin and eosin (H&E), Masson, and immunohistochemistry for IL-6, TNF-α, VEGF, and CD34.

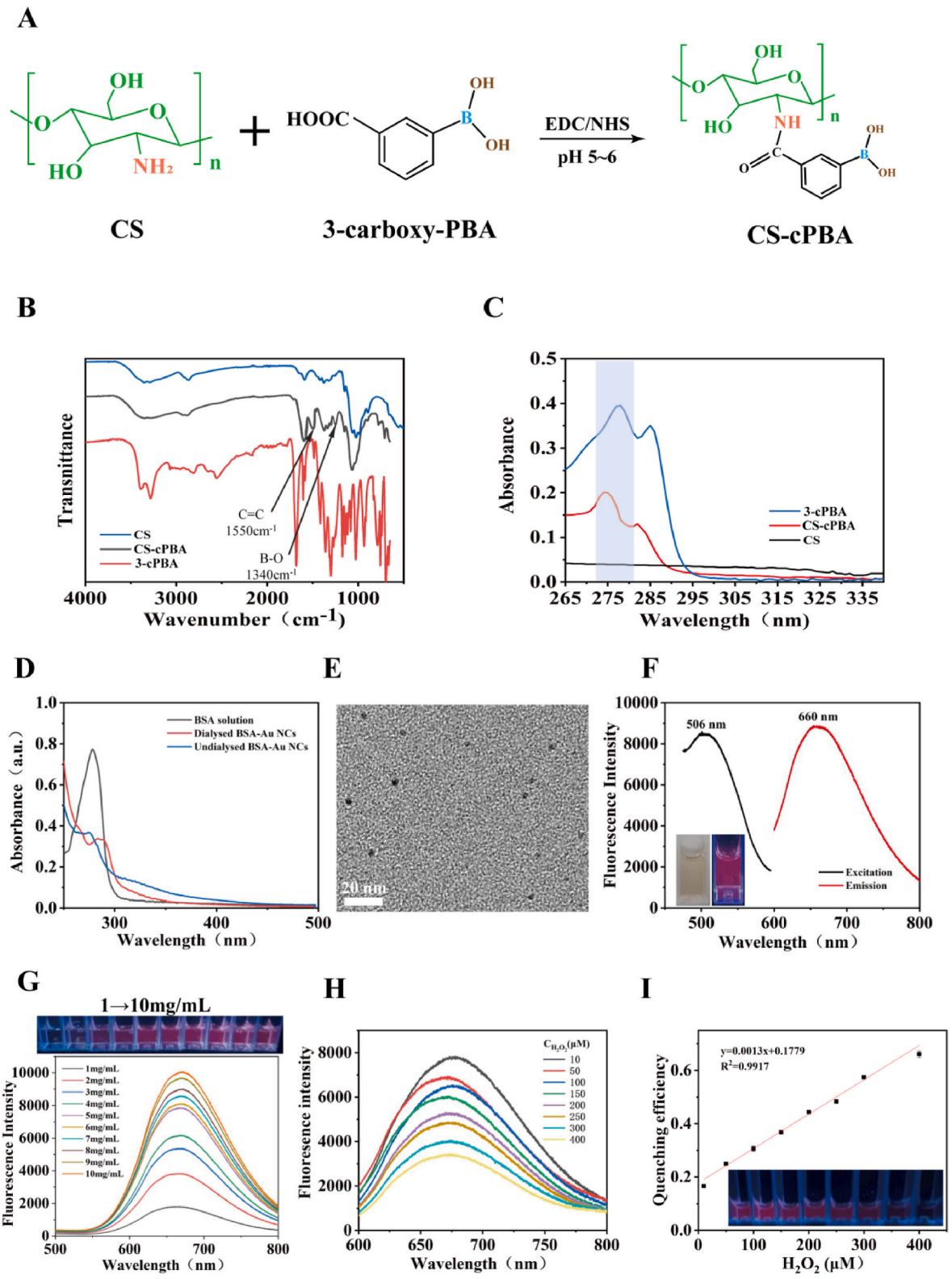

Fig. 1. Characterization of CS-cPBA and BSA-Au NCs. (A) CS-cPBA molecule synthesis process. (B) Fourier transform infrared (FTIR) spectra and (C) UV–vis spectra of CS, 3-cPBA, and CS-cPBA molecules. (D) UV–vis spectra for BSA, BSA-Au NCs (before and after dialysis). (E) TEM image of BSA-Au NCs. (F) Fluorescence excitation (black curve) and emission (red curve) spectra of BSA-Au NCs. Insets are the images of BSA-Au NCs solution under daylight and UV light. (G) Fluorescence intensity with different concentrations of BSA-Au NCs (1–10 mg/ml). Insets showed the corresponding fluorescence images under ultraviolet light. (H) Fluorescence spectra and (I) linearity graph of BSA-Au NCs (5 mg/mL) incubated with different concentrations of hydrogen peroxide (10–400 μM). Insets showed the corresponding fluorescence images under ultraviolet light.

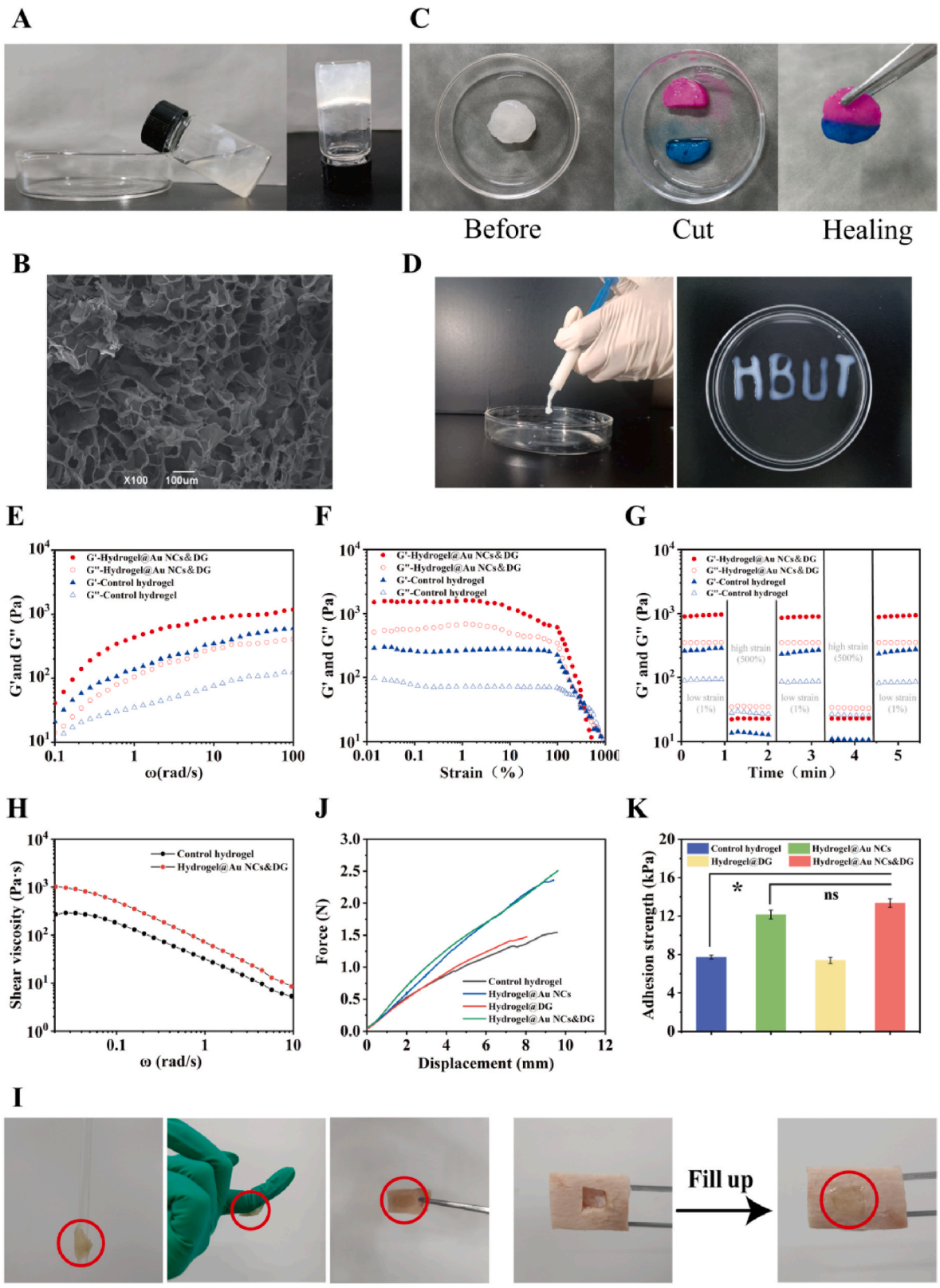

Fig. 2. Multifunctional properties of hydrogels. (A) Gel transition process of Control hydrogel. (B) SEM of Control hydrogel. (C) Self-healing process of Control hydrogel. (D) Injectable property of Control hydrogel. (E) Frequency dependence of storage (G′) and loss (G″) modulus, (F) oscillatory strain sweep, (G) self-healing performance and (H) shear viscosity of hydrogels. (I) Adhesion of Hydrogel@Au NCs&DG on various substrates, such as glass, rubber, and tissue (red circles mean Hydrogel@Au NCs&DG). (J) Adhesion force and (K) adhesion strength of hydrogels.

2.10. Statistical analysis

The statistical difference was analyzed by one-way ANOVA. The difference of $P < 0.05$ is considered statistically significant ($P < 0.05$ (*), $P < 0.01$ (**) and $P < 0.001$ (***)).

3. Results and discussion

3.1. Preparation and characterization of CS-cPBA, BSA-Au NCs

Chitosan (CS) with good biocompatibility, biodegradability, and low toxicity was selected to fabricate hydrogel. In order to endow hydrogel with self-healing function by reversible dynamic bonds, chitosan was modified first with 3-carboxy phenylboronic acid by forming an amide bond (Fig. 1A). The successfully prepared CS-cPBA was verified by FTIR and UV–vis absorbance. As shown in Fig. 1B, two peaks at 1500~1690 cm^{-1} and 1310~1350 cm^{-1} were observed, which ascribed to the skeleton vibration of benzene ring with C═C and the stretching vibration of borate bond with B–O, respectively [43,44]. In the UV–vis absorption spectra, there was an absorption peak similar to 3-cPBA at about 275 nm, indicating that 3-cPBA was successfully grafted onto CS (Fig. 1C) [45]. The grafting rate of 3-cPBA on CS was calculated to be about 57.49 ± 2.6 % by comparing with the UV–vis absorbance (ABS) standard curve of 3-cPBA at 275 nm (Fig. S1).

Next, BSA-Au NCs were synthesized by a facile method under mild conditions. Under alkaline conditions, Au^{3+} was reduced to gold atoms by aromatic amino acids in BSA molecules, and cysteine residues in BSA molecules play an important role in the stable synthesis of gold nanoclusters [46]. In UV–vis spectra, an absorption peak was observed at about 280 nm, which could be attributed to the peptide bond of bovine serum albumin (Fig. 1D, black curve). The absorption peak around 280 nm of BSA-Au NCs after dialysis confirmed that BSA was tightly covered on the surface of Au NCs [37]. TEM examination revealed that the average size of BSA-Au NCs was about 3 nm (Fig. 1E), and the hydrated particle size was about 140 nm (Fig. S2A). Importantly, the as-prepared BSA-Au NCs solution showed bright red fluorescence under ultraviolet light with the maximum emission wavelength (λem) of 660 nm under the excitation wavelength (λex) of 506 nm (Fig. 1F).

The fluorescence intensity of BSA-Au NCs with different concentrations (1–10 mg/mL, Fig. 1G) was investigated. With the increase in the concentration of BSA-Au NCs, the fluorescence intensity gradually increased while the cell viability gradually decreased (Fig. S2B). Furthermore, when the concentration of BSA-Au NCs increased from 5 mg/mL to 10 mg/mL, there was no obvious difference in fluorescence images (inserts in Fig. 1G). The time stability of the reaction between BSA-Au NCs and H_2O_2 was also studied. As shown in Fig. S2C, when the reaction time was about 20 min, it had reached the plateau. Hence, the subsequent experiments were carried out at the BSA-Au NCs concentration of 5 mg/mL and the detection time of H_2O_2 was set as 20 min at pH = 7.4. Subsequently, the response of BSA-Au NCs to different concentrations of H_2O_2 (10–400 μM) was detected. It was observed that with the increase of H_2O_2, the fluorescence intensity of BSA-Au NCs decreased gradually (Fig. 1H and I), and there was a linear relationship between fluorescence quenching efficiency of BSA-Au NCs and hydrogen peroxide concentration. The results indicated that BSA-Au NCs can be employed for the quantitative detection of hydrogen peroxide.

3.2. Preparation, characterization, and mechanical properties of hydrogel

Chitosan modified with boric acid (CS-cPBA) was mixed with β-GP solution to form hydrogel about 10 s (Fig. 2A, Video. S1). It was also confirmed by the dynamic time scanning rheological analysis (Fig. S3). The microstructure of the hydrogel was characterized by scanning electron microscope first. As shown in Fig. 2B, the Control hydrogel showed a uniform porous structure with a pore size of 100–200 μm. When the hydrogel was loaded with DG alone, the pore size did not change obviously (Fig. S4A), but when the hydrogel was loaded with BSA-Au NCs, the pore size decreased obviously (Figs. S4B, C, D). It may be attributed to the cross linking of protein molecules in BSA-Au NCs with the hydrogel. Element Mapping showed that Au and K atoms were uniformly distributed in the Hydrogel@Au NCs&DG, indicating that BSA-Au NCs and DG were loaded (Fig. S4E). The above results were further verified by the XPS spectrum (Fig. S5). Finally, we investigated the effects of different loadings of BSA-Au NCs and DG on the gelation time and injectability of the hydrogel. It was found that the amount of BSA-Au NCs and DG had little effect on the formation of hydrogel (Table S1).

Next, the self-healing and injectable functions of Control hydrogel were investigated. As shown in Fig. 2C, the circular hydrogel was cut into two parts. Then the incisions of the two parts dyed with different colors were fixed together again. After 30 min, it was observed that the two parts were successfully healed together, and they could not be separated using tweezers. By transferring the hydrogel into a syringe and then extruding it, the letter "HBUT" could be formed (Fig. 2D), demonstrating the Control hydrogel with good self-healing and injectable properties.

In order to examine the mechanical properties of the hydrogel, frequency scanning, and strain scanning were carried out to evaluate the energy storage (G′) and loss modulus (G ″) of hydrogel. As shown in Fig. 2E and S6A, under the constant strain of 0.5 %, the storage modulus of all hydrogels was greater than the loss modulus in the frequency range of 0.1–100 rad/s, which suggested the formation of gels. At the same time, it was observed that the storage modulus and loss modulus of the hydrogels loaded with BSA-Au NCs were higher than those of the blank hydrogel and the hydrogel loaded with DG. It could be put down to the fact that the hydrogels loaded with BSA-Au NCs enhanced their mechanical properties due to their denser structure. Fig. 2F and S6B showed that when the applied strain exceeds 500 %, the G′ was lower than the G″, because the structure was destroyed. Therefore, in the subsequent self-healing measurement experiments, the strain was set from 1 % to 500 %. It was observed that the hydrogels' structure was destroyed at 500 % strain, but it returned to the gel state at 1 % strain, which proved that these hydrogels had good self-healing performance (Fig. 2G and S6C). Reversible borate bonds can endow hydrogels with shear thinning and injectability, so we measured the shear thinning ability of hydrogels. As shown in Fig. 2H and S6D, the viscosity of hydrogels decreased with the increase of shear rate, showing normal shear thinning ability. The shear thinning ability of the Hydrogel@Au NCs&DG group was higher than that of the Control hydrogel group, indicating that the mechanical properties of Hydrogel@Au NCs&DG group were enhanced. Finally, the adhesive properties of hydrogels were measured. As shown in Fig. 2I and S6E, the adhesive behaviors of Hydrogel@Au NCs&DG and Hydrogel@Au NCs on rubber gloves, glass rods, porcine skin, and porcine skin tissue were tested. The results revealed that Hydrogel@Au NCs&DG and Hydrogel@Au NCs had good adhesive property, while the Control hydrogel and Hydrogel@DG had low adhesive property. The tissue-adhesiveness of the hydrogel on porcine skin tissues was also measured to obtain the force-displacement graphs (Fig. 2J). The adhesion strength of the hydrogel group containing BSA-Au NCs was about 12~13 kPa, while that of the hydrogel group without BSA-Au NCs was only about 7 kPa, further confirming good adhesive property of Hydrogel@Au NCs&DG and Hydrogel@Au NCs (Fig. 2K). It may be because BSA, as a natural globular protein, can attach itself to almost all soft or hard surfaces, thus giving hydrogel adhesion [47]. In addition, the amino and carboxyl groups on the skin could form hydrogen bonds with BSA to enhance the adhesion [48,49].

3.3. Swelling and drug release behavior of hydrogel

An ideal wound dressing should provide a moist microenvironment for the wound and absorb a large amount of exudate, and these depend on the swelling rate of hydrogel [39]. Therefore, the swelling ability of

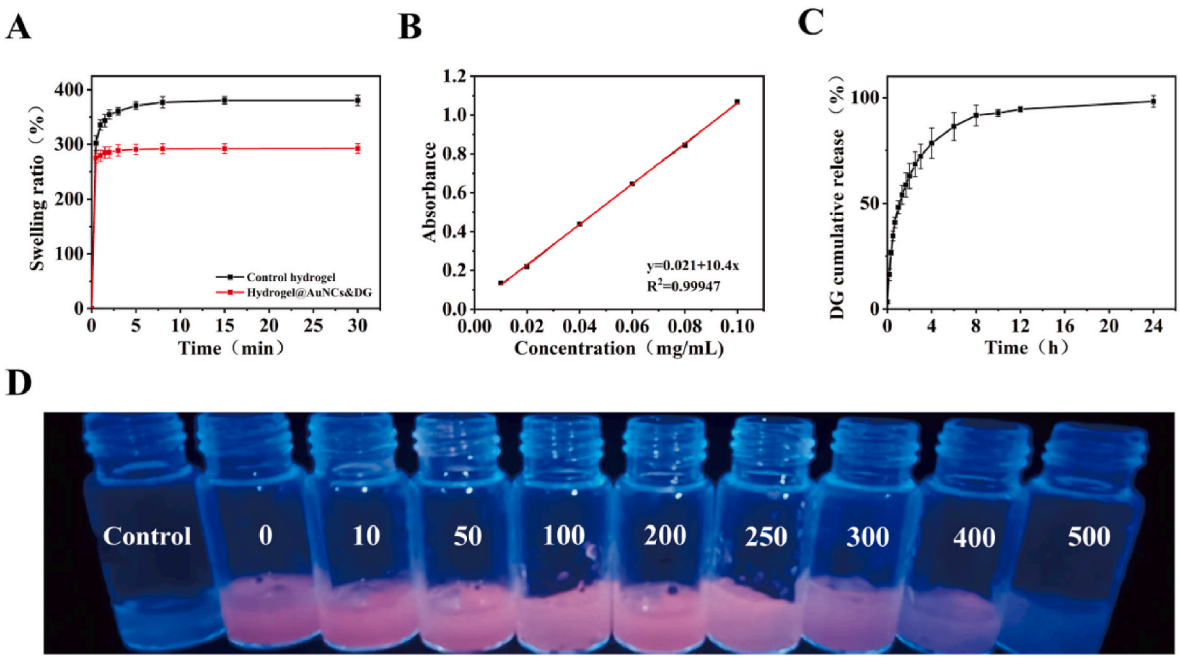

Fig. 3. Swelling and drug release properties of hydrogels. (A) Swelling behavior of the Control hydrogel and Hydrogel@Au NCs&DG in PBS. (B) Standard curve of DG. (C) The in vitro DG release property of the Hydrogel@Au NCs&DG in PBS with pH 7.4 at 37 °C. (D) The image of fluorescence quenching of Hydrogel@Au NCS&DG at different concentrations of H_2O_2 (0–500 μM).

hydrogels in physiological environment was tested. As shown in Fig. 3A and S6F, the Control hydrogel and Hydrogel@DG swelled rapidly within 5 min, and reached the swelling balance within half an hour with the swelling rate as high as about 380 %. The swelling rates of Hydrogel@Au NCs and Hydrogel@Au NCs&DG were about 290 %. It was probably due to the decrease in pore size of Hydrogel@Au NCs and thus led to the decrease in swelling performance. This was also consistent with the results of SEM. DG could be used to treat inflammatory reaction during wound healing. The release of DG from hydrogel was calculated according to the standard curve (Fig. 3B). Fig. 3C showed that DG could be released up to 100 % after 24 h, implying the hydrogel was suitable for the treatment of wounds with inflammation. Subsequently, the fluorescence quenching effect of H_2O_2 on Hydrogel@Au NCs&DG was tested. The results showed that the fluorescence of the Hydrogel@Au NCs&DG decreased with the increase of H_2O_2, indicating that the as-prepared hydrogels could be employed to monitor the concentration of H_2O_2 (Fig. 3D). Apart from this, we found that the swelling of hydrogel had little effect on its fluorescence (Fig. S7).

3.4. Hydrogel biocompatibility and cell scratch healing

The ideal wound dressing should be biocompatible. In order to evaluate the biocompatibility of hydrogels, blood and cell compatibility experiments were carried out. The results showed that the hemolysis rate of each hydrogel group was lower than 5 %, indicating each hydrogel exhibited good blood compatibility (Fig. 4A and B). For cell compatibility, mouse fibroblast L929 cells were co-cultured with the extract of hydrogel material, and after 24 h, the cells were double stained to distinguish between living cells and dead cells. As shown in Fig. 4C–a large number of green living cells and a small number of red dead cells were observed in each hydrogel group. MTT assay was used to detect the toxicity of hydrogel to L929 cells. Firstly, we tested the cell compatibility of Hydrogel@Au NCs&DG at different concentrations. It was found that the cell survival rate of the as-prepared hydrogel was up to 80 % at the concentrations of 1 g/mL after 24h incubation (Fig. S8). Then we tested the cell toxicity of hydrogels with different components at the concentration of 1 g/mL. Compared with the blank group, each hydrogel group had a weak effect on cell viability, which confirmed that hydrogel had good cell compatibility (Fig. 4D). Next, the cell scratch experiment was used to simulate wound healing in vitro. In order to simulate the inflammation of wound surface, L929 cells were pretreated with lipopolysaccharide (LPS) [43]. As shown in Fig. 4E, both Hydrogel@DG group and Hydrogel@Au NCs&DG group had obvious cell migration effects, and the cell migration rate of Hydrogel@Au NCs&DG group reached up to 90 % at 36 h (Fig. 4F). It may be due to the sustained releasing of anti-inflammatory drugs which inhibited cell inflammatory reaction and promoted cell migration.

3.5. Anti-inflammatory properties of hydrogel in vitro

Treatment of inflammation is usually achieved by inhibiting proinflammatory cytokine tumor necrosis factor (TNF)-α and promoting the expression of anti-inflammatory factor interleukin (IL)-10 [50,51]. Lipopolysaccharide (LPS) can stimulate macrophages through nuclear factor pathway translocation and induce macrophages to secrete inflammatory factors [52]. In order to simulate the inflammatory environment, macrophages are induced by LPS first. Fig. 5A showed that the cell survival rates of the Hydrogel@DG group and Hydrogel@Au NCs&DG group were significantly higher than those of the LPS group after 12 h and 24 h incubation, indicating successful fabrication of inflammatory environment. Next, the expressions of TNF-α and IL-10 were quantitatively detected by enzyme-linked immunosorbent assay (ELISA) kits. As shown in Fig. 5B and C, the Hydrogel@DG group and Hydrogel@Au NCs&DG group had obvious effects of promoting IL-10 and inhibiting TNF-α expression. It was attributed to the sustained release of anti-inflammatory drugs which reduced the inflammatory response of macrophages.

3.6. Evaluation of wound healing performance in vivo

In order to explore hydrogel-mediated wound healing in vivo, Kunming mice were used to construct a round wound model with a diameter of 1 cm. The experiment was divided into six groups, named Control, Hydrosorb gel (Commercial hydrogel), Control hydrogel,

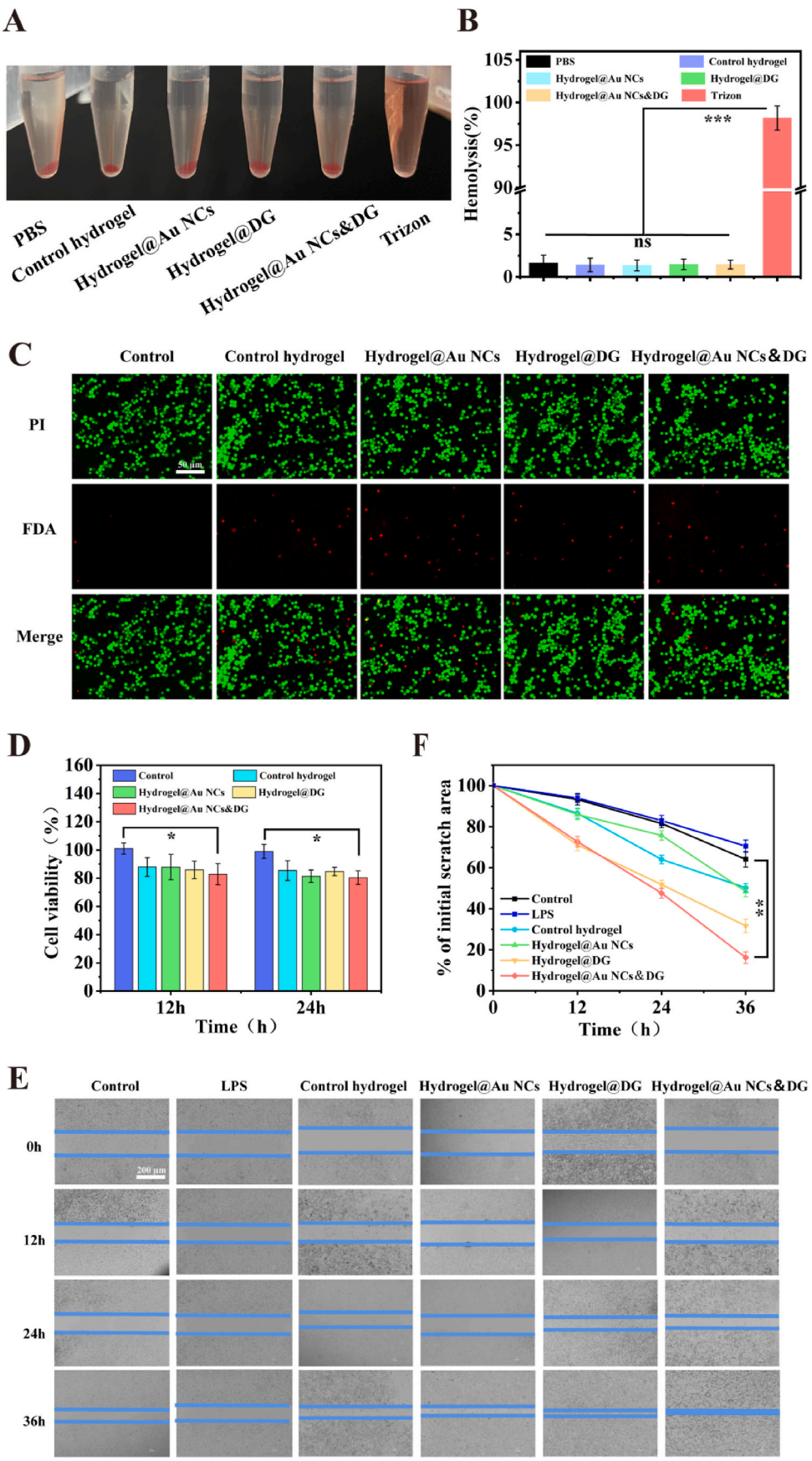

Fig. 4. Biocompatibility and cell migration ability evaluation in vitro. (A) Image of the hemolysis assay and (B) hemolysis ratio of different hydrogels. (C) Live/dead cell imaging of L929 cells treated with different hydrogels for 24h. All scale bars are 50 μm. (D) L929 cell viability after the treatment of different hydrogels for 12 and 24 h. (E) Photographs of L929 cell migration at different times and (F) quantitative results. All scale bars are 200 μm.

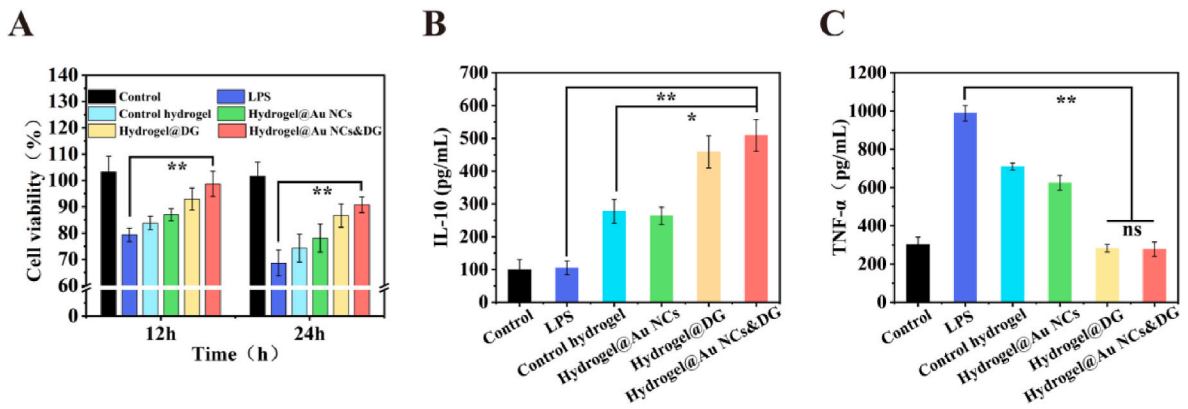

Fig. 5. Anti-inflammatory properties of hydrogels in vitro. (A) Cell viability of macrophages mediated by different hydrogels after LPS induction. (B) IL-10 and (C) TNF-α were detected by the enzyme-linked immunosorbent assay (ELISA).

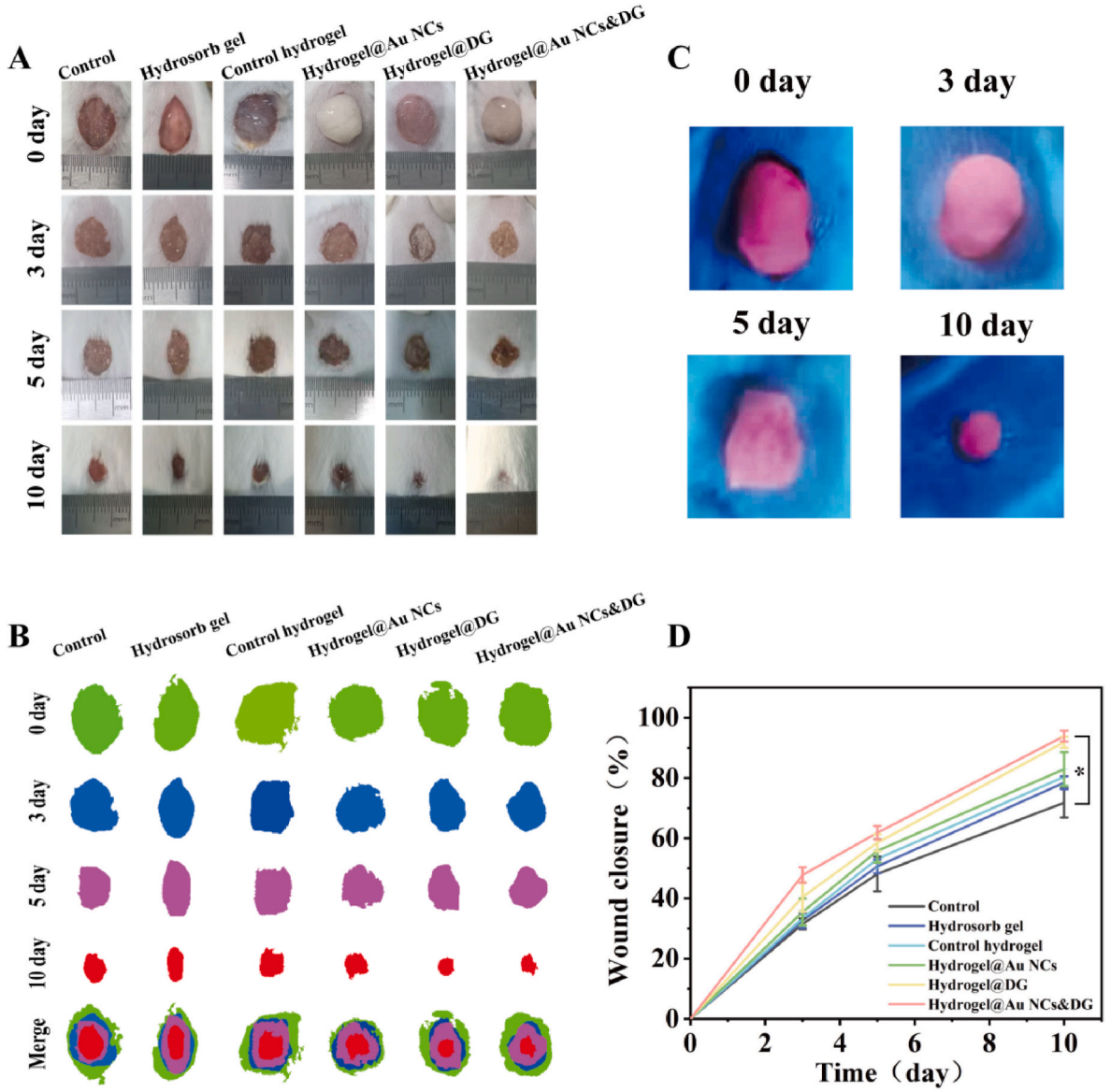

Fig. 6. Assessment of hydrogel in vivo wound treatment. (A) Images of wound healing at different times. (B) The simulated changes in wound size during 10 days. (C) Fluorescent photos at different times under ultraviolet lamp irradiation. (D) Quantitative graph of wound healing.

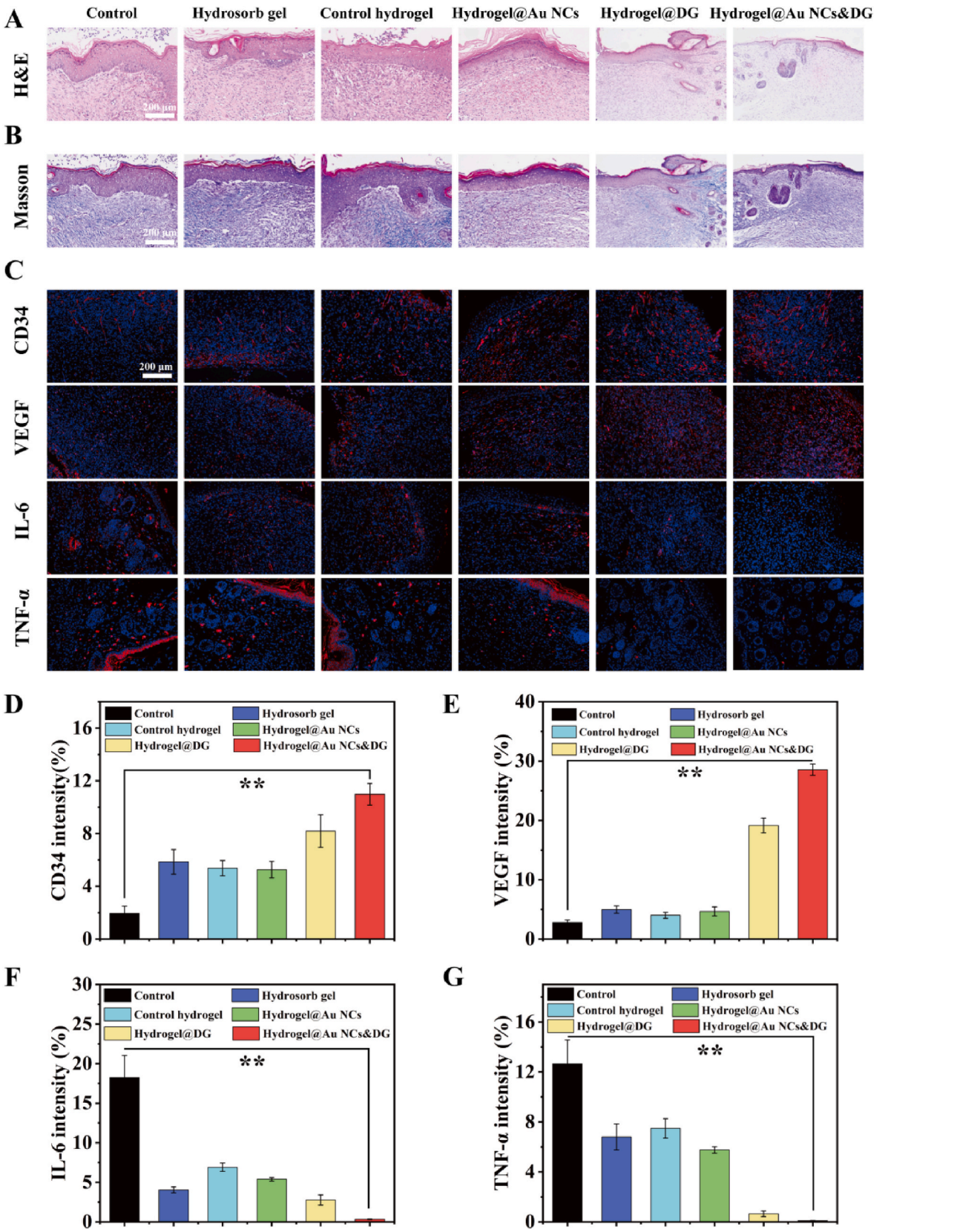

Fig. 7. Histological evaluation of wound tissues after the treatment of 10 days. Images of (A) H&E staining and (B) Masson's staining on the 10th day. (C) CD34, VEGF, IL-6, and TNF-α immunofluorescence staining (red) on the 10th day. The scale bar is 200 μm. Quantitative fluorescence intensity map of (D) CD34, (E) VEGF, (F) IL-6, and (G) TNF-α.

Hydrogel@Au NCs, Hydrogel@DG and Hydrogel@Au NCs&DG. The images of wound healing (Fig. 6A and B) showed that the Hydrogel@Au NCs&DG group with good adhesive property could promote wound healing compared with other groups. The wound usually went through the stage of hemostasis first, then the body's autoimmune or bacterial infection produced an inflammatory response [23]. Thus, Hydrogel@Au NCs&DG had a bright red fluorescence when the wound was first formed. On days 3 and 5, the fluorescence of Hydrogel@Au NCs&DG was quenched due to the production of an inflammatory response and the release of hydrogen peroxide. After 10 days of treatment, the inflammation disappeared, the wound healed, and the fluorescence of Hydrogel@Au NCs&DG was bright (Fig. 6C). Moreover, the healing rate of the Hydrogel@Au NCs&DG group was significantly faster than that of other groups. Concretely, on the 3rd and the 5th day, for the as-prepared hydrogel, the wound healing area decreased by about 43 % and 60 %, respectively. By the 10th day, the healing rate reached about 90 % and the wound healed almost completely (Fig. 6D). The above results proved that the as-prepared Hydrogel@Au NCs&DG could promote wound healing and reflect the wound inflammation change further guide the use of wound dressing.

3.7. Histological evaluation of wound healing

The wound tissue on the 10th day was sliced to further evaluate the wound healing. According to the results of hematoxylin-eosin (H&E) staining of wound tissue, the thickness of epidermis in the Hydrogel@Au NCs&DG group was obviously thinner than that of other control groups. As the process of re-epithelization is the transition from immature thick epithelium to mature thin epithelium [53], the above results indicated that the re-epithelization in the Hydrogel@Au NCs&DG group was better. In addition, more dense granulation tissue and new hair follicles could be observed in the Hydrogel@DG group and Hydrogel@Au NCs&DG group further demonstrating the good recovery of the wound (Fig. 7A). Collagen is the main extracellular matrix component in dermis, which can reflect the degree of wound repair. Masson staining was used to evaluate the collagen deposition of the wound. It showed that the collagen deposition in the Hydrogel@Au NCs&DG group was denser and more regular than that in other control groups (Fig. 7B). The wound tissue was stained with fluorescent markers of vascular endothelial cell (CD34) and angiogenesis factor (VEGF) to observe the angiogenesis of the wound surface. Compared with other groups, the Hydrogel@Au NCs&DG group showed more angiogenesis (Fig. 7C, D, E), and sufficient blood vessels would bring nutrients and oxygen to the wound, thus promoting wound healing. Finally, the wound tissue was stained by immunohistochemistry [42]. As shown in Fig. 7C–F, G, the IL-6 and TNF-α stained images of each control group showed a large number of inflammatory factors, while the Hydrogel@Au NCs&DG group showed a low inflammatory response. It can be concluded that the hydrogel of Hydrogel@Au NCs&DG group can reduce the production of inflammatory cells and down-regulate the pro-inflammatory factors TNF-α and IL-10, thus regulating the inflammatory reaction, promoting the growth of granulation tissue and wound healing.

4. Conclusions

In summary, we have developed an injectable smart hydrogel for wound inflammation monitoring and treatment by visual fluorescent color change and release of anti-inflammatory drugs. The Hydrogel@Au NCs&DG is formed by connecting boric acid modified chitosan with β-GP through boric acid ester bond and hydrogen bond. As the boric acid ester bond is a reversible dynamic bond, the as-prepared hydrogel is endowed with self-healing and injectable ability. The combination of BSA-Au NCs can not only detect the hydrogen peroxide produced by wound inflammation but also increase the adhesion of the hydrogel due to the existence of bovine serum albumin. In vivo studies show that the addition of the anti-inflammatory drug DG can reduce the production of inflammatory cells, accelerate the growth of granulation tissue, and promote wound healing. The Hydrogel@Au NCs&DG with good biocompatibility and low biological toxicity has a good application prospect in inflammation detection and wound healing.

CRediT authorship contribution statement

Yunjing Jiang: Writing – review & editing, Writing – original draft, Software, Methodology, Data curation, Conceptualization. **Yuyu Cao:** Software, Data curation. **Jie Wu:** Data curation. **Rongxian Bai:** Data curation. **Shufan Wan:** Investigation. **Lei Dai:** Investigation. **Jiangtao Su:** Resources, Project administration. **Hongmei Sun:** Writing – review & editing, Writing – original draft, Validation, Supervision, Resources, Project administration, Conceptualization.

Declaration of competing interest

The authors declare that they have no known competing financial interests or personal relationships that could have appeared to influence the work reported in this paper.

Data availability

Data will be made available on request.

Acknowledgement

This work was supported by the HBUT National "111″ Center for Cellular Regulation and Molecular Pharmaceutics (No. XBTK-2022007).

Appendix A. Supplementary data

Supplementary data to this article can be found online at https://doi.org/10.1016/j.mtbio.2024.100960.

References

[1] G. Eke, N. Mangir, N. Hasirci, S. MacNeil, V. Hasirci, Development of a UV crosslinked biodegradable hydrogel containing adipose derived stem cells to promote vascularization for skin wounds and tissue engineering, Biomaterials 129 (2017) 188–198, https://doi.org/10.1016/j.biomaterials.2017.03.021.
[2] J.I. Kang, K.M. Park, Advances in gelatin-based hydrogels for wound management, J. Mater. Chem. B 9 (6) (2021) 1503–1520, https://doi.org/10.1039/d0tb02582h.
[3] R. Dong, B. Guo, Smart wound dressings for wound healing, Nano Today 41 (2021), https://doi.org/10.1016/j.nantod.2021.101290.
[4] J. Xia, H. Zhang, F. Yu, Y. Pei, X. Luo, Superclear, porous cellulose membranes with chitosan-coated nanofibers for visualized cutaneous wound healing dressing, ACS Appl. Mater. Interfaces 12 (21) (2020) 24370–24379, https://doi.org/10.1021/acsami.0c05604.
[5] G.D. Nicodemus, S.J. Bryant, Cell encapsulation in biodegradable hydrogels for tissue engineering applications, Tissue Eng., Part B 14 (2) (2008) 149–165, https://doi.org/10.1089/ten.teb.2007.0332.
[6] J.S. Boateng, K.H. Matthews, H.N. Stevens, G.M. Eccleston, Wound healing dressings and drug delivery systems: a review, J. Pharmaceut. Sci. 97 (8) (2008) 2892–2923, https://doi.org/10.1002/jps.21210.
[7] Q. Liang, Z. Shen, X. Sun, D. Yu, K. Liu, S.M. Mugo, W. Chen, D. Wang, Q. Zhang, Electron conductive and transparent hydrogels for recording brain neural signals and neuromodulation, Adv. Mater. 35 (9) (2023) e2211159, https://doi.org/10.1002/adma.202211159.
[8] J. Wang, Y. Chen, G. Zhou, Y. Chen, C. Mao, M. Yang, Polydopamine-coated Antheraea pernyi (A. pernyi) silk fibroin films promote cell adhesion and wound healing in skin tissue repair, ACS Appl. Mater. Interfaces 11 (38) (2019) 34736–34743, https://doi.org/10.1021/acsami.9b12643.
[9] L. Qi, C. Zhang, B. Wang, J. Yin, S. Yan, Progress in hydrogels for skin wound repair, Macromol. Biosci. 22 (7) (2022) e2100475, https://doi.org/10.1002/mabi.202100475.
[10] M. Hosseini, M. Amiri, M. Ghanbari, M.A. Mahdi, W.K. Abdulsahib, M. Salavati-Niasari, Drug delivery based on chitosan, β-cyclodextrin and sodium carboxymethyl cellulose as well as nanocarriers for advanced leukemia treatment, Biomed. Pharmacother. 153 (2022), https://doi.org/10.1016/j.biopha.2022.113369.
[11] M. Kong, X.G. Chen, K. Xing, H.J. Park, Antimicrobial properties of chitosan and mode of action: a state of the art review, Int. J. Food Microbiol. 144 (1) (2010) 51–63, https://doi.org/10.1016/j.ijfoodmicro.2010.09.012.

[12] Z. Guo, R. Chen, R. Xing, S. Liu, H. Yu, P. Wang, C. Li, P. Li, Novel derivatives of chitosan and their antifungal activities in vitro, Carbohydr. Res. 341 (3) (2006) 351–354, https://doi.org/10.1016/j.carres.2005.11.002.
[13] M.W. Tm, W.M. Lau, V.V. Khutoryanskiy, Chitosan and its derivatives for application in mucoadhesive drug delivery systems, Polymers 10 (3) (2018), https://doi.org/10.3390/polym10030267.
[14] B. Sheokand, M. Vats, A. Kumar, C.M. Srivastava, I. Bahadur, S.R. Pathak, Natural polymers used in the dressing materials for wound healing: past, present and future, J. Polym. Sci. 61 (14) (2023) 1389–1414, https://doi.org/10.1002/pol.20220734.
[15] J. Tang, W. Yi, J. Yan, Z. Chen, H. Fan, D. Zaldivar-Silva, L. Aguero, S. Wang, Highly absorbent bio-sponge based on carboxymethyl chitosan/poly-gamma-glutamic acid/platelet-rich plasma for hemostasis and wound healing, Int. J. Biol. Macromol. 247 (2023) 125754, https://doi.org/10.1016/j.ijbiomac.2023.125754.
[16] R. Dong, X. Zhao, B. Guo, P.X. Ma, Self-healing conductive injectable hydrogels with antibacterial activity as cell delivery carrier for cardiac cell therapy, ACS Appl. Mater. Interfaces 8 (27) (2016) 17138–17150, https://doi.org/10.1021/acsami.6b04911.
[17] Y. Liang, J. He, B. Guo, Functional hydrogels as wound dressing to enhance wound healing, ACS Nano 15 (8) (2021) 12687–12722, https://doi.org/10.1021/acsnano.1c04206.
[18] S. Geng, H. Zhao, G. Zhan, Y. Zhao, X. Yang, Injectable in situ forming hydrogels of thermosensitive polypyrrole nanoplatforms for precisely synergistic photothermo-chemotherapy, ACS Appl. Mater. Interfaces 12 (7) (2020) 7995–8005, https://doi.org/10.1021/acsami.9b22654.
[19] H. Qin, J. Wang, T. Wang, X. Gao, Q. Wan, X. Pei, Preparation and characterization of chitosan/beta-glycerophosphate thermal-sensitive hydrogel reinforced by graphene oxide, Front. Chem. 6 (2018) 565, https://doi.org/10.3389/fchem.2018.00565.
[20] H.Y. Zhou, L.J. Jiang, P.P. Cao, J.B. Li, X.G. Chen, Glycerophosphate-based chitosan thermosensitive hydrogels and their biomedical applications, Carbohydr. Polym. 117 (2015) 524–536, https://doi.org/10.1016/j.carbpol.2014.09.094.
[21] T. Huang, Y. Cao, Y. Jiang, B. Zhai, R. Bai, J. Wu, X. You, H. Sun, Analysis of Antimicrobial and Wound-Healing Properties of Injectable and Adhesive Thermosensitive Hydrogels with Ultrafast Self-gelling, Chin. J. Anal. Chem. 51 (2023) 982–993, https://doi.org/10.19756/j.issn.0253-3820.231142.
[22] C. Huang, L. Dong, B. Zhao, Y. Lu, S. Huang, Z. Yuan, G. Luo, Y. Xu, W. Qian, Anti-inflammatory hydrogel dressings and skin wound healing, Clin. Transl. Med. 12 (11) (2022) e1094, https://doi.org/10.1002/ctm2.1094.
[23] T. Velnar, T. Bailey, V. Smrkolj, The wound healing process: an overview of the cellular and molecular mechanisms, J. Int. Med. Res. 37 (5) (2009) 1528–1542, https://doi.org/10.1177/147323000903700531.
[24] S.S. Ramasastry, Acute wounds, Clin. Plast. Surg. 32 (2) (2005) 195–208, https://doi.org/10.1016/j.cps.2004.12.001.
[25] A.E. Loo, Y.T. Wong, R. Ho, M. Wasser, T. Du, W.T. Ng, B. Halliwell, Effects of hydrogen peroxide on wound healing in mice in relation to oxidative damage, PLoS One 7 (11) (2012) e49215, https://doi.org/10.1371/journal.pone.0049215.
[26] A. van der Vliet, Y.M. Janssen-Heininger, Hydrogen peroxide as a damage signal in tissue injury and inflammation: murderer, mediator, or messenger? J. Cell. Biochem. 115 (3) (2014) 427–435, https://doi.org/10.1002/jcb.24683.
[27] M. Hu, K. Korschelt, P. Daniel, K. Landfester, W. Tremel, M.B. Bannwarth, Fibrous nanozyme dressings with catalase-like activity for H(2)O(2) reduction to promote wound healing, ACS Appl. Mater. Interfaces 9 (43) (2017) 38024–38031, https://doi.org/10.1021/acsami.7b12212.
[28] S. Schreml, M. Landthaler, M. Schaferling, P. Babilas, A new star on the H(2)O(2) rizon of wound healing? Exp. Dermatol. 20 (3) (2011) 229–231, https://doi.org/10.1111/j.1600-0625.2010.01195.x.
[29] Q. Huang, Y. Yang, Y. Zhu, Q. Chen, T. Zhao, Z. Xiao, M. Wang, X. Song, Y. Jiang, Y. Yang, J. Zhang, Y. Xiao, Y. Nan, W. Wu, K. Ai, Oral metal-free melanin nanozymes for natural and durable targeted treatment of inflammatory bowel disease (IBD), Small 19 (19) (2023) e2207350, https://doi.org/10.1002/smll.202207350.
[30] J. Kanta, The role of hydrogen peroxide and other reactive oxygen species in wound healing, Acta Med. 54 (3) (2011).
[31] G. Zhu, Q. Wang, S. Lu, Y. Niu, Hydrogen peroxide: a potential wound therapeutic target? Med. Princ. Pract. 26 (4) (2017) 301–308, https://doi.org/10.1159/000475501.
[32] K. Korschelt, M.N. Tahir, W. Tremel, A step into the future: applications of nanoparticle enzyme mimics, Chemistry 24 (39) (2018) 9703–9713, https://doi.org/10.1002/chem.201800384.
[33] J. Wu, X. Wang, Q. Wang, Z. Lou, S. Li, Y. Zhu, L. Qin, H. Wei, Nanomaterials with enzyme-like characteristics (nanozymes): next-generation artificial enzymes (II), Chem. Soc. Rev. 48 (4) (2019) 1004–1076, https://doi.org/10.1039/c8cs00457a.
[34] Z. Bai, G. Li, J. Liang, J. Su, Y. Zhang, H. Chen, Y. Huang, W. Sui, Y. Zhao, Non-enzymatic electrochemical biosensor based on Pt NPs/RGO-CS-Fc nano-hybrids for the detection of hydrogen peroxide in living cells, Biosens. Bioelectron. 82 (2016) 185–194, https://doi.org/10.1016/j.bios.2016.04.004.
[35] D. Rojas, J.F. Hernandez-Rodriguez, F. Della Pelle, M. Del Carlo, D. Compagnone, A. Escarpa, Oxidative stress on-chip: Prussian blue-based electrode array for in situ detection of H(2)O(2) from cell populations, Biosens. Bioelectron. 170 (2020) 112669, https://doi.org/10.1016/j.bios.2020.112669.
[36] S. Song, Y. Liu, A. Song, Z. Zhao, H. Lu, J. Hao, Peroxidase mimetic activity of Fe(3)O(4) nanoparticle prepared based on magnetic hydrogels for hydrogen peroxide and glucose detection, J. Colloid Interface Sci. 506 (2017) 46–57, https://doi.org/10.1016/j.jcis.2017.07.029.
[37] V. Jain, S. Bhagat, S. Singh, Bovine serum albumin decorated gold nanoclusters: a fluorescence-based nanoprobe for detection of intracellular hydrogen peroxide, Sensor. Actuator. B Chem. 327 (2021), https://doi.org/10.1016/j.snb.2020.128886.
[38] C.D.S. Leite, O.C. Pires, D.G. Tenis, J.V.N. Ziegler, D.G. Priolli, T. Rocha, Effects of dipotassium glycyrrhizinate on wound healing, Acta Cir. Bras. 36 (8) (2021) e360801, https://doi.org/10.1590/ACB360801.
[39] D.Y. Zhu, Z.P. Chen, Z.P. Hong, L. Zhang, X. Liang, Y. Li, X. Duan, H. Luo, J. Peng, J. Guo, Injectable thermo-sensitive and wide-crack self-healing hydrogel loaded with antibacterial anti-inflammatory dipotassium glycyrrhizate for full-thickness skin wound repair, Acta Biomater. 143 (2022) 203–215, https://doi.org/10.1016/j.actbio.2022.02.041.
[40] D. Zhang, Q. Ouyang, Z. Hu, S. Lu, W. Quan, P. Li, Y. Chen, S. Li, Catechol functionalized chitosan/active peptide microsphere hydrogel for skin wound healing, Int. J. Biol. Macromol. 173 (2021) 591–606, https://doi.org/10.1016/j.ijbiomac.2021.01.157.
[41] Y.Z. Jianping Xie, Jackie Y. Ying*, Protein-directed synthesis of highly fluorescent gold nanoclusters, J. Am. Chem. Soc. 131 (3) (2009) 888–889.
[42] Y. Liu, K. Ai, X. Cheng, L. Huo, L. Lu, Gold-nanocluster-based fluorescent sensors for highly sensitive and selective detection of cyanide in water, Adv. Funct. Mater. 20 (6) (2010) 951–956, https://doi.org/10.1002/adfm.200902062.
[43] C. Hu, F. Zhang, L. Long, Q. Kong, R. Luo, Y. Wang, Dual-responsive injectable hydrogels encapsulating drug-loaded micelles for on-demand antimicrobial activity and accelerated wound healing, J. Contr. Release 324 (2020) 204–217, https://doi.org/10.1016/j.jconrel.2020.05.010.
[44] Z. Lyu, S. Sun, T. Wu, Highly stretchable covalent adaptive networks enabled by dynamic boronic diester linkages with nitrogen→boron coordination, J. Polym. Sci. 60 (1) (2021) 72–80, https://doi.org/10.1002/pol.20210706.
[45] Y. Wang, Y. Wu, L. Long, L. Yang, D. Fu, C. Hu, Q. Kong, Y. Wang, Inflammation-Responsive drug-loaded hydrogels with sequential hemostasis, antibacterial, and anti-inflammatory behavior for chronically infected diabetic wound treatment, ACS Appl. Mater. Interfaces 13 (28) (2021) 33584–33599, https://doi.org/10.1021/acsami.1c09889.
[46] M.L. Cui, J.M. Liu, X.X. Wang, L.P. Lin, L. Jiao, L.H. Zhang, Z.Y. Zheng, S.Q. Lin, Selective determination of cysteine using BSA-stabilized gold nanoclusters with red emission, Analyst 137 (22) (2012) 5346–5351, https://doi.org/10.1039/c2an36284h.
[47] Z. Tang, Q. Chen, F. Chen, L. Zhu, S. Lu, B. Ren, Y. Zhang, J. Yang, J. Zheng, General principle for fabricating natural globular protein-based double-network hydrogels with integrated highly mechanical properties and surface adhesion on solid surfaces, Chem. Mater. 31 (1) (2018) 179–189, https://doi.org/10.1021/acs.chemmater.8b03860.
[48] W. Liu, R. Xie, J. Zhu, J. Wu, J. Hui, X. Zheng, F. Huo, D. Fan, A temperature responsive adhesive hydrogel for fabrication of flexible electronic sensors, npj Flexible Electronics 6 (1) (2022), https://doi.org/10.1038/s41528-022-00193-5.
[49] Y. Jiang, X. Zhang, W. Zhang, M. Wang, L. Yan, K. Wang, L. Han, X. Lu, Infant skin friendly adhesive hydrogel patch activated at body temperature for bioelectronics securing and diabetic wound healing, ACS Nano 16 (6) (2022) 8662–8676, https://doi.org/10.1021/acsnano.2c00662.
[50] R.C. Coll, A.A. Robertson, J.J. Chae, S.C. Higgins, R. Munoz-Planillo, M.C. Inserra, I. Vetter, L.S. Dungan, B.G. Monks, A. Stutz, D.E. Croker, M.S. Butler, M. Haneklaus, C.E. Sutton, G. Nunez, E. Latz, D.L. Kastner, K.H. Mills, S.L. Masters, K. Schroder, M.A. Cooper, L.A. O'Neill, A small-molecule inhibitor of the NLRP3 inflammasome for the treatment of inflammatory diseases, Nat. Med. 21 (3) (2015) 248–255, https://doi.org/10.1038/nm.3806.
[51] S. Papoutsopoulou, L. Pollock, C. Walker, W. Tench, S.S. Samad, F. Bergey, L. Lenzi, R. Sheibani-Tezerji, P. Rosenstiel, M.T. Alam, V.A.P. Martins Dos Santos, W. Muller, B.J. Campbell, Impact of interleukin 10 deficiency on intestinal epithelium responses to inflammatory signals, Front. Immunol. 12 (2021) 690817, https://doi.org/10.3389/fimmu.2021.690817.
[52] E. Schilling, R. Weiss, A. Grahnert, M. Bitar, U. Sack, S. Hauschildt, Molecular mechanism of LPS-induced TNF-alpha biosynthesis in polarized human macrophages, Mol. Immunol. 93 (2018) 206–215, https://doi.org/10.1016/j.molimm.2017.11.026.
[53] Q. Li, S. Zhang, R. Du, Y. Yang, Y. Liu, Z. Wan, X. Yang, Injectable self-healing adhesive natural glycyrrhizic acid bioactive hydrogel for bacteria-infected wound healing, ACS Appl. Mater. Interfaces 15 (14) (2023) 17562–17576, https://doi.org/10.1021/acsami.2c23231.